Journal of Statistical Physics, Vol. 115, Nos. 5/6, June 2004 (© 2004)

Lévy Flights in a Steep Potential Well

Aleksei V. Chechkin,[1] Vsevolod Yu. Gonchar,[1] Joseph Klafter,[2] Ralf Metzler,[3] and Leonid V. Tanatarov[1]

Received June 20, 2003; accepted January 8, 2004

Lévy flights in steeper than harmonic potentials have been shown to exhibit finite variance and a critical time at which a bifurcation from an initial monomodal to a terminal bimodal distribution occurs (Chechkin *et al.*, *Phys. Rev. E* **67**:010102(R) (2003)). In this paper, we present a detailed study of Lévy flights in potentials of the type $U(x) \propto |x|^c$ with $c > 2$. Apart from the bifurcation into bimodality, we find the interesting result that for $c > 4$ a trimodal transient exists due to the temporal overlap between the decay of the central peak around the initial δ-condition and the building up of the two emerging side-peaks, which are characteristic for the stationary state. Thus, for certain system parameters there exists a transient trimodal distribution of the Lévy flight. These properties of Lévy flights in external potentials of the power-law type can be represented by certain phase diagrams. We also present details about the proof of multimodality and the numerical procedures to establish the probability distribution of the process.

KEY WORDS: Random walks and Lévy flights; stochastic processes; classical transport; stochastic analysis methods (Fokker–Planck, Langevin, etc.).

1. INTRODUCTION

Lévy flights (LFs) are stochastic, Markov processes, which differ from regular Brownian motion by the occurrence of extremely long jumps, whose length is distributed according to a Lévy stable law with the long tail $\sim |x|^{-1-\alpha}$, such that its second moment diverges.[1–5] This property strongly contrasts the classical Gaussian description of diffusion processes which possess finite moments of any given order.[6, 7] Given their Markov nature,

[1] Institute for Theoretical Physics NSC KIPT, Akademicheskaya st. 1, 61108 Kharkov, Ukraine.
[2] School of Chemistry, Tel Aviv University, 69978 Tel Aviv, Israel.
[3] NORDITA, Blegdamsvej 17, DK-2100 Copenhagen Ø, Denmark; e-mail: metz@nordita.dk

0022-4715/04/0600-1505/0 © 2004 Plenum Publishing Corporation

the divergence of the variance of an LF might disqualify them as physically meaningful model processes for diffusing particles with a finite mass. Yet, LFs have important applications to processes, in which no finite velocity is required, such as in the energy diffusion in single molecule spectroscopy.[8] An impressive experimental evidence of Lévy processes was reported by the group of Walther in the study of the position of a single ion in a one-dimensional optical lattice, in which diverging fluctuations could be observed in the kinetic energy.[9] From a phenomenological point of view, LFs have been used to describe the dynamics observed in plasmas[10] or in molecular collisions.[11] They have also been successfully applied to describe the statistics encountered in the spatial gazing patterns of bacteria,[12] albatross birds,[13] or even spidermonkeys.[14] Probably the earliest application of LFs, however, may be in the modelling of financial markets.[15] LFs were shown to give rise to surprisingly rich band structures in periodic potentials.[16] Reverse engineering methods have been developed to construct a Langevin system with Lévy noise to produce a pre-defined steady state.[17] We also note that the stationary state of LFs in a confining external potential is expected to approach to the one of Lévy walks for long times[18, 19] (the spatiotemporally coupled version of LFs which have converging moments of any order), and therefore the more straightforward determination of the solution for LFs might be used to gain insight into Lévy walks.

The theory of homogeneous LFs is well understood: Thus, LFs in the continuum limit can, inter alia, be described by continuous time random walks with long-tailed, asymptotic power-law jump length distributions,[18] or alternatively by a Langevin equation with δ-correlated, Lévy noise.[20–22] Both descriptions can be mapped onto the (space-) fractional diffusion equation[21, 23–26]

$$\frac{\partial f}{\partial t} = D \frac{\partial^{\alpha}}{\partial |x|^{\alpha}} f(x, t), \tag{1}$$

where the fractional Riesz operator $\partial^{\alpha}/\partial |x|^{\alpha}$ is most easily defined in terms of its Fourier transform[27]

$$\int_{-\infty}^{\infty} e^{ikx} \frac{\partial^{\alpha}}{\partial |x|^{\alpha}} f(x, t)\, dx \equiv -|k|^{\alpha} \hat{f}(k, t); \tag{2}$$

here, $0 < \alpha \leqslant 2$. In the following we restrict our analysis to the range $1 \leqslant \alpha \leqslant 2$. In the limit $\alpha = 2$, naturally, Eq. (1) reduces to the classical diffusion equation, which describes Gaussian transport. From the Fourier

transform of Eq. (1), $\partial f/\partial t = -D\,|k|^{\alpha}\,\hat{f}(k,t)$, we conclude that the characteristic function is

$$\hat{f}(k,t) = \exp(-Dt\,|k|^{\alpha}), \tag{3}$$

i.e., exactly the characteristic function of a symmetric Lévy stable law of index α.[3,4] In position space, expression (3) can be represented exactly in terms of Fox H-functions,[25,28] but for our purposes in what follows, it is enough to remember that for large $|x|$, we find $f(x,t) \sim Dt/|x|^{1+\alpha}$, such that the variance diverges: $\langle x^2(t)\rangle = \infty$. Also the general formulation of LFs in external potentials and in phase space seems well founded, in terms of fractional Klein–Kramers equations; see, e.g., refs. 24, 29–31.

However, much less is known about the actual behaviour of LFs in external potentials $U(x)$, i.e., about the properties of the probability density function (PDF) $f(x,t)$ in the presence of such a $U(x)$. One of the few solved examples is the one of LFs in a harmonic potential,[32] whose solution always follows the same stable law of index α, like in the regular Ornstein–Uhlenbeck process the PDF always stays Gaussian. In general, LFs in the presence of an external potential field in the overdamped case are governed by the (space-) fractional Fokker–Planck (or Einstein–Smoluchowski) equation[21,23–25]

$$\frac{\partial f}{\partial t} = \left(\frac{\partial}{\partial x}\frac{U'(x)}{m\eta} + D\,\frac{\partial^{\alpha}}{\partial\,|x|^{\alpha}}\right) f(x,t), \tag{4}$$

which has the characteristic property that the drift term enters with the usual first order derivative and thus preserves its additive quality such that for a constant force $F(x) = Vm\eta$ the solution is given by the drift-free PDF taken at the similarity variable $x - Vt$, and for a general external potential the stationary solution differs from the Boltzmann distribution. This latter property is in contrast to an alternative LF model suggested in ref. 33.

An unexpected behaviour of LFs was obtained recently as solution of the fractional Fokker–Planck equation (4), namely the occurrence of bimodal solutions (PDFs with two maxima) and the finiteness of the second moment in the presence of superharmonic potentials of the form[34,35]

$$U(x) = \frac{ax^{2m+2}}{2m+2}, \qquad m = 1, 2, \ldots . \tag{5}$$

Note that the amplitude $a > 0$ has dimension $[a] = \mathrm{g}\cdot\mathrm{cm}^{-2m}/\mathrm{sec}^2$. Thus, for a potential of the form $U(x) = ax^2 + bx^4$ with $a, b > 0$, a turnover can be tuned from the properties of the solution of the harmonic problem

(monomodal/unimodal, diverging variance) to a finite variance and bimodal solution by varying the ratio b/a.[35] If such bimodality occurs, it results from a bifurcation at a critical time t_c.[35] A typical result is shown in Fig. 1, for the quartic case $m = 1$ and Lévy index $\alpha = 1.2$: from an initial δ-peak, eventually a bimodal distribution emerges. Note that we use dimensionless quantities in the plots, as introduced below. The location of the global maximum/maxima is displayed in Fig. 2, where the bifurcation is a distinct mark. In the same figure, the value of the PDF f at the newly emerging humps is compared to the value at the origin.

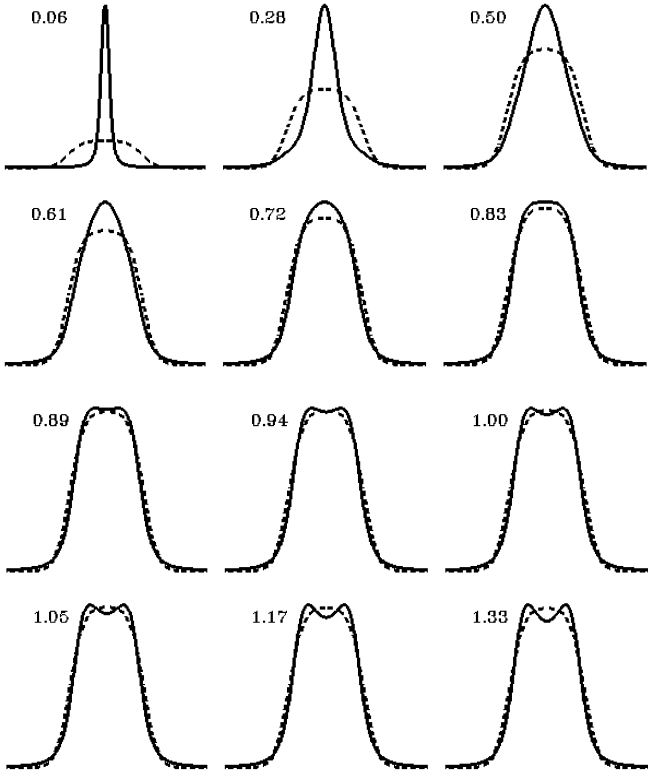

Fig. 1. Time evolution of the LF-PDF in the presence of the superharmonic external potential (5) with $c = 4$ (quartic Lévy oscillator) and Lévy index $\alpha = 1.2$, obtained from the numerical solution of the fractional Fokker–Planck equation, using the Grünwald–Letnikov representation of the fractional Riesz derivative (full line). The initial condition is a δ-function at the origin. The dashed lines indicate the corresponding Boltzmann distribution. The transition from one to two maxima is clearly seen. This picture of the time evolution is typical for $2 < c \leqslant 4$ see below. The corresponding location of the maximum/maxima as a function of time is shown in Fig. 2.

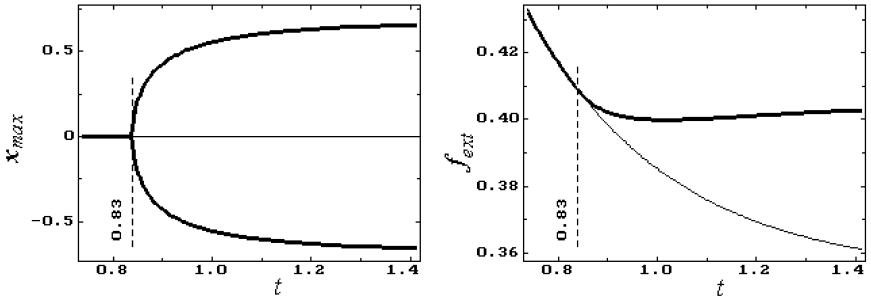

Fig. 2. Bifurcation diagrams for the case $c = 4.0$, $\alpha = 1.2$, corresponding to the PDF shown in Fig. 1. Left: the thick lines show the location of the maximum, which at the bifurcation time $t_{12} = 0.84 \pm 0.01$ turns into two maxima. Right: the value of the PDF in the maxima location (thick line) and the value in the minimum at $x = 0$ (thin line).

In what follows, we briefly review the description of LFs in external fields in terms of the Langevin equation with white Lévy noise and the space-fractional Fokker–Planck equation, as well as the properties of LFs in superharmonic potentials; and we present two proofs, for both the finite variance in these cases and the existence of multimodality. We then proceed to show that for potentials steeper than (5) with $m = 1$, even a trimodal PDF can be obtained. In two phase diagrams, we can classify the existence of the different n-modal states in dependence of the potential exponent c and the Lévy index α; and the critical bifurcations between different n-modal domains as a function of time t and potential exponent c. In the appendix, we discuss the numerical methods from which the PDFs are obtained.

2. STARTING EQUATIONS

In this section, we formulate the dynamical description of LFs on the stochastic differential (Langevin equation) and the deterministic (fractional Fokker–Planck equation) levels. For the latter, we also discuss the corresponding form in Fourier space.

2.1. Starting Equations in Real Space

2.1.1. The Langevin Equation with Lévy Noise

On the level of the stochastic description, our starting point is the overdamped Langevin equation[20, 21, 38]

$$\frac{dx}{dt} = \frac{F(x)}{M\gamma} + Y_\alpha(t), \tag{6}$$

where $F = -dU/dx$ is an external force with potential

$$U(x) = \frac{a\,|x|^c}{c}, \tag{7}$$

with $a > 0$ and $c \geqslant 2$, M is the particle mass, γ the friction coefficient, and $Y_\alpha(t)$ represents a stationary white Lévy noise with Lévy index α ($1 \leqslant \alpha \leqslant 2$).

We employ the white Lévy noise $Y_\alpha(t)$ such that the process

$$L(\Delta t) = \int_t^{t+\Delta t} Y_\alpha(\tau)\, d\tau, \tag{8}$$

i.e., the time integral over an increment Δt, is an α-stable process with stationary independent increments. Restricting ourselves to symmetric Lévy laws, this implies the characteristic function

$$\hat{p}_L(k, \Delta t) = \exp(-D\,|k|^\alpha\,\Delta t). \tag{9}$$

The constant D in this description has the meaning of the intensity of the Langevin source, and $[D] = \mathrm{cm}^\alpha/\mathrm{sec}$.

In Fig. 3, we show realisations of white Lévy noises for various values of α. The sharply pronounced "outliers," due to the long-tailed nature of the Lévy stable distribution, are distinct, in comparison to the Gaussian case $\alpha = 2$.

2.1.2. Fractional Fokker–Planck Equation

The Langevin equation (6) is still of the Markov-type, and it is therefore fairly straightforward to show that the corresponding fluctuation-averaged (deterministic) description is given in terms of the space-fractional Fokker–Planck equation (4).[20, 21, 34] In what follows, we derive the solution of Eq. (4) for the δ-initial condition

$$f(x, 0) = \delta(x). \tag{10}$$

The space-fractional derivative $\partial^\alpha/\partial|x|^\alpha$ occurring in the fractional Fokker–Planck equation (4) is called the Riesz fractional derivative, defined through

$$\frac{d^\alpha f}{d|x|^\alpha} = \begin{cases} -\dfrac{\mathbf{D}_+^\alpha f + \mathbf{D}_-^\alpha f}{2\cos(\pi\alpha/2)}, & \alpha \neq 1 \\ -\dfrac{d}{dx}\mathbf{H}f, & \alpha = 1, \end{cases} \tag{11}$$

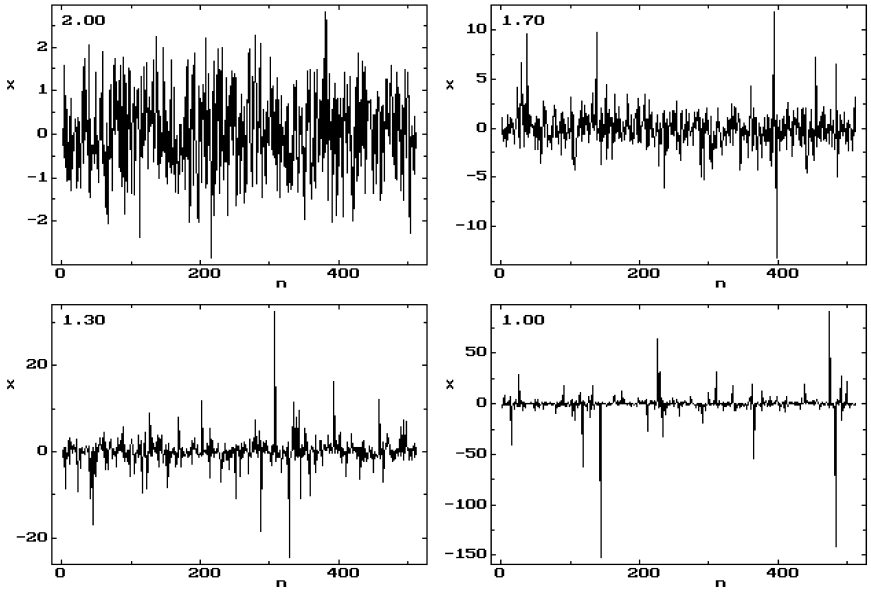

Fig. 3. White Lévy noises with the Lévy indexes $\alpha = 2, 1.7, 1.3, 1.0$. The "outliers" are increasingly more pronounced the smaller the Lévy index α becomes. Note the different scales on the ordinates.

where we use the following abbreviations:

$$(\mathbf{D}_+^\alpha f)(x) = \frac{1}{\Gamma(2-\alpha)} \frac{d^2}{dx^2} \int_{-\infty}^{x} \frac{f(\xi, t)\, d\xi}{(x-\xi)^{\alpha-1}}, \tag{12}$$

and

$$(\mathbf{D}_-^\alpha f)(x) = \frac{1}{\Gamma(2-\alpha)} \frac{d^2}{dx^2} \int_{x}^{\infty} \frac{f(\xi, t)\, d\xi}{(\xi-x)^{\alpha-1}} \tag{13}$$

for, respectively, the left and right Riemann–Liouville derivatives ($1 \leqslant \alpha < 2$); and[36]

$$(\mathbf{H}f)(x) = \frac{1}{\pi} \int_{-\infty}^{\infty} \frac{f(\xi)\, d\xi}{x-\xi} \tag{14}$$

is the Hilbert transform. Note that the integral is to be interpreted as the principal value. The definitions for $\partial^\alpha / \partial |x|^\alpha$ demonstrate the strongly nonlocal property of the space-fractional Fokker–Planck equation, i.e., strong correlations in x.

2.1.3. Rescaling of the Dynamical Equations

Passing to dimensionless variables

$$x' = x/x_0, \qquad t' = t/t_0, \tag{15}$$

with

$$x_0 = \left(\frac{MD\gamma}{a}\right)^{1/(c-2+\alpha)}, \qquad t_0 = \frac{x_0^\alpha}{D}, \tag{16}$$

the starting equations take the form (we omit primes below)

$$\frac{dx}{dt} = -\frac{dU}{dx} + Y_\alpha(t) \tag{17}$$

instead of the Langevin equation (6), and

$$\frac{\partial f(x,t)}{\partial t} = \frac{\partial}{\partial x}\frac{dU}{dx} f + \frac{\partial^\alpha f}{\partial |x|^\alpha} \tag{18}$$

instead of the fractional Fokker–Planck equation (4), and

$$U(x) = \frac{|x|^c}{c}. \tag{19}$$

2.2. Starting Equations in Fourier Space

If $\hat{f}(k,t)$ denotes the characteristic function (CF), i.e., Fourier transform of $f(x,t)$, we write

$$f(x,t) \div \hat{f}(k,t), \tag{20}$$

where we use the sign $\div$ to denote a Fourier transform pair. Since[27]

$$(\mathbf{D}_\pm^\alpha f)(x,t) \div (\mp ik)^\alpha \hat{f}(k,t), \tag{21}$$

and

$$(\mathbf{H} f)(x,t) \div i\,\mathrm{sign}(k)\,\hat{f}(k,t), \tag{22}$$

we obtain

$$\frac{\partial^\alpha f}{\partial |x|^\alpha} \div -|k|^\alpha \hat{f}(k,t), \tag{23}$$

for all α's. The equivalent of the fractional Fokker–Planck equation (18) for the CF then follows immediately,

$$\frac{\partial \hat{f}}{\partial t} + |k|^{\alpha} \hat{f} = \mathsf{U}_k \hat{f}, \tag{24}$$

with the initial condition

$$\hat{f}(k, t = 0) = 1, \tag{25}$$

and the normalisation

$$\hat{f}(k = 0, t) = 1. \tag{26}$$

The external potential $U(x)$ turns into the linear differential operator in k,

$$\begin{aligned} \mathsf{U}_k \hat{f} &= \int_{-\infty}^{\infty} e^{ikx} \frac{\partial}{\partial x} \left(\frac{dU}{dx} f \right) dx \\ &= -ik \int_{-\infty}^{\infty} e^{ikx} \operatorname{sign}(x) \, |x|^{c-1} \, f(x, t) \, dx. \end{aligned} \tag{27}$$

Next, making use of the following "inverse" expressions

$$(\pm ix)^{\alpha} f(x) \div (\mathbf{D}_{\pm}^{\alpha} \hat{f})(k), \tag{28}$$

and

$$-i(\operatorname{sign}(x) \, f(x) \div (\mathbf{H} \hat{f})(k), \tag{29}$$

we obtain the explicit expression for the external potential operator,

$$\mathsf{U}_k \hat{f} = \begin{cases} \dfrac{k}{2 \cos(\pi c/2)} (\mathbf{D}_{+}^{c-1} - \mathbf{D}_{-}^{c-1}) \, \hat{f}, & c \neq 3, 5, 7, \ldots \\ (-1)^m \, k \dfrac{d^{2m}}{dk^{2m}} \mathbf{H} \hat{f}, & c = 3, 5, 7, \ldots . \end{cases} \tag{30}$$

Note that for the even potential exponents $c = 2m+2$, $m = 0, 1, 2, \ldots$, we find the simplified expression

$$\mathsf{U}_k = (-1)^{m+1} \, k \frac{\partial^{2m+1}}{\partial k^{2m+1}}, \tag{31}$$

in terms of regular derivatives in k. We see that the force term can be written in terms of fractional derivatives in Fourier space, and therefore it is not straightforward to calculate even the stationary solution of the fractional Fokker–Planck equation (18) in the general case $c \notin \mathbb{N}$. In particular, in this latter case, the nonlocal Eq. (18) in x-space translates into a nonlocal equation in k-space, where the nonlocality shifts from the diffusion to the drift term.

3. ANALYTICAL RESULTS

In the preceding section, we discussed some elementary properties of the space-fractional Fokker–Planck equation for LFs, in particular, we pointed out the spatially nonlocal character of Eq. (18), and its Fourier space counterpart (24). In this section, we determine the analytical solution of the fractional Fokker–Planck equation. We start with the exactly solvable stationary quartic Cauchy oscillator, to demonstrate directly the occurring bimodality, and then move on to the general case. The major results will be the determination of n-modality, finite variance, and the parametric dependence of the associated bifurcations.

3.1. The Stationary Quartic Cauchy Oscillator

Let us first regard the case of the stationary quartic potential with $c = 4$ for the Cauchy-LF with $\alpha = 1$, i.e., the solution of the equation

$$\frac{d}{dx} x^3 f_{\mathrm{st}}(x) + \frac{d}{d|x|} f_{\mathrm{st}}(x) = 0, \tag{32}$$

or,

$$\frac{d^3 \hat{f}_{\mathrm{st}}(k)}{dk^3} = \mathrm{sign}(k)\, |k|\, \hat{f}_{\mathrm{st}}(k) \tag{33}$$

in Fourier space. Its solution is

$$\hat{f}_{\mathrm{st}}(k) = \frac{2}{\sqrt{3}} \exp\left(-\frac{|k|}{2}\right) \cos\left(\frac{\sqrt{3}\,|k|}{2} - \frac{\pi}{6}\right), \tag{34}$$

whose inverse Fourier transform results in the simple analytical form

$$f_{\mathrm{st}}(x) = \frac{1}{\pi(1 - x^2 + x^4)}. \tag{35}$$

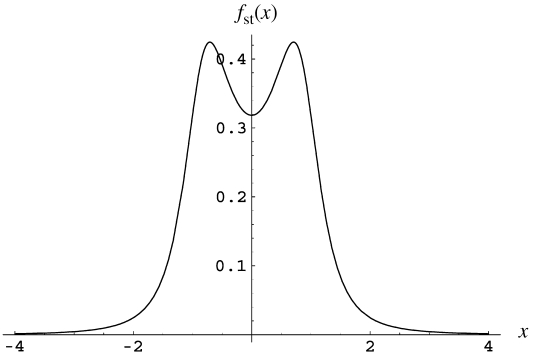

Fig. 4. Stationary PDF (35) of the Cauchy-LF in a quartic ($c=4$) potential. Two global maxima exist at $x_{\max}=\pm\sqrt{1/2}$, and there is a local minimum at the origin.

As shown in Fig. 4, this solution has *two global maxima* at $x_{\max}=\pm 1/\sqrt{2}$ apart from a local minimum at the origin (the position of the initial condition, that is) and its variance

$$\langle x^2\rangle = 1 \tag{36}$$

is *finite*, due to the long-tail asymptotics $f_{st}(x)\sim x^{-4}$. These two distinct properties for LFs will turn out to be a central theme in the remainder of this work.

3.2. Formal Solution of Eq. (18)

Returning to the general case, we rewrite Eq. (24) in the equivalent integral form,

$$\hat{f}(k,t)=\hat{p}_\alpha(k,t)+\int_0^t d\tau\ \hat{p}_\alpha(k,t-\tau)\ \mathsf{U}_k\hat{f}(k,\tau) \tag{37}$$

where

$$\hat{p}_\alpha(k,t)=\exp(-|k|^\alpha t) \tag{38}$$

is the CF of a free (homogeneous) LF. This relation follows from Eq. (24) via formally treating it as a nonhomogeneous linear differential equation of first order, where U_k plays the role of the nonhomogeneity. Then, (24) is obtained from variation of constants. (Differentiate Eq. (37) to return to (24).)

Equation (37) can be solved formally by iterations: Let

$$\hat{f}^{(0)}(k, t) = \hat{p}_\alpha(k, t), \tag{39}$$

then

$$\hat{f}^{(1)}(k, t) = \hat{p}_\alpha(k, t) + \int_0^t d\tau\, \hat{p}_\alpha(k, t-\tau)\, \mathsf{U}_k \hat{f}^{(0)}(k, \tau), \tag{40}$$

$$\hat{f}^{(2)}(k, t) = \hat{p}_\alpha(k, t) + \int_0^t d\tau\, \hat{p}_\alpha(k, t-\tau)\, \mathsf{U}_k \hat{p}_\alpha(k, \tau) + \int_0^t d\tau \int_0^\tau d\tau'\, \hat{p}_\alpha(k, t-\tau)\, \mathsf{U}_k \hat{p}_\alpha(k, \tau-\tau')\, \mathsf{U}_k \hat{p}_\alpha(k, \tau'), \tag{41}$$

etc. Invoking the definition of the convolution,

$$A * B = \int_0^t d\tau\, A(t-\tau)\, B(\tau) = \int_0^t d\tau\, A(\tau)\, B(t-\tau), \tag{42}$$

and using

$$A * B * C = (A * B) * C = A * (B * C), \tag{43}$$

we arrive at the formal solution

$$\hat{f}(k, t) = \sum_{n=0}^{\infty} \hat{p}_\alpha (* \mathsf{U}_k \hat{p}_\alpha)^n. \tag{44}$$

This procedure is analogous to perturbation theory, $\mathsf{U}_k \hat{f}$ playing the role of the interaction term, see, for instance, ref. 37, Chapter 16.

Applying a Laplace transformation,

$$\tilde{\hat{f}}(k, s) = \int_0^\infty dt \exp(-st)\, \hat{f}(k, t), \tag{45}$$

to Eq. (37), we obtain

$$\tilde{\hat{f}}(k, s) = \tilde{\hat{p}}_\alpha(k, s) + \tilde{\hat{p}}_\alpha(k, s)\, \mathsf{U}_k \tilde{\hat{f}}(k, s), \tag{46}$$

where

$$\tilde{\hat{p}}_\alpha(k, s) = \frac{1}{s + k^\alpha} \tag{47}$$

is the Fourier–Laplace transform of the homogeneous Lévy stable PDF (note that $\tilde{\hat{p}}(k, s)$ is even in k). Thus, we obtain the equivalent of solution (44) in (k, s)-space:

$$\tilde{\tilde{f}}(k, s) = \sum_{n=0}^{\infty} [\tilde{\hat{p}}_\alpha(k, s)\, \mathsf{U}_k]^n\, \tilde{\hat{p}}_\alpha(k, s). \tag{48}$$

This iterative construction scheme for the solution of the fractional Fokker–Planck equation will turn out to be useful below.

3.3. Existence of a Bifurcation Time

For the case of the unimodal initial condition $f(x, 0) = \delta(x)$ we now prove the existence of a finite bifurcation time t_{12} for the turnover from unimodal to bimodal PDF. At this time, the curvature at the origin will vanish, i.e., be an inflection point:

$$\left.\frac{\partial^2 f}{\partial x^2}\right|_{x=0,\, t=t_{12}} = 0. \tag{49}$$

Introducing

$$J(t) = \int_0^\infty dk\, k^2 \hat{f}(k, t), \tag{50}$$

Eq. (49) is equivalent to (note that the CF is an even function)

$$J(t_{12}) = 0. \tag{51}$$

The bifurcation can now be obtained from the iterative solution (48); we consider the specific case $c = 4$. From the first order approximation

$$\tilde{\tilde{f}}_1(k, s) = \frac{1}{s + k^\alpha}\left(1 + \mathsf{U}_k \frac{1}{s + k^\alpha}\right), \tag{52}$$

and we have

$$\mathsf{U}_k = k \frac{\partial^3}{\partial k^3}. \tag{53}$$

Combining these two expressions, we produce

$$\tilde{\hat{f}}_1(k,s) = \frac{1}{s+k^\alpha} + \alpha(\alpha-1)(2-\alpha)\frac{k^{\alpha-2}}{(s+k^\alpha)^3} + 6\alpha^2(\alpha-1)\frac{k^{2\alpha-2}}{(s+k^\alpha)^4} - 6\alpha^3\frac{k^{3\alpha-2}}{(s+k^\alpha)^5}, \tag{54}$$

or, after inverse Laplace transformation,

$$\hat{f}_1(k,t) = e^{-k^\alpha t}\left\{1 - \frac{\alpha^3}{4}t^4k^{3\alpha-2} + \alpha^2(\alpha-1)\,t^3k^{2\alpha-2} + \alpha(\alpha-1)(2-\alpha)\frac{t^2}{2}k^{\alpha-2}\right\}. \tag{55}$$

The first approximation to the bifurcation time t_{12} is then determined via Eq. (50), i.e., we calculate

$$\int_0^\infty dk\, k^2 \hat{f}_1(k, t_{12}^{(1)}) = 0, \tag{56}$$

to obtain

$$t_{12}^{(1)} = \left(\frac{4\Gamma(3/\alpha)}{3(3-\alpha)\,\Gamma(1/\alpha)}\right)^{\alpha/(2+\alpha)}. \tag{57}$$

In Fig. 5, we show the dependence of this first approximation $t_{12}^{(1)}$ as a function of the Lévy index α (dashed line), in comparison to the values determined from the numerical solution of the fractional Fokker–Planck

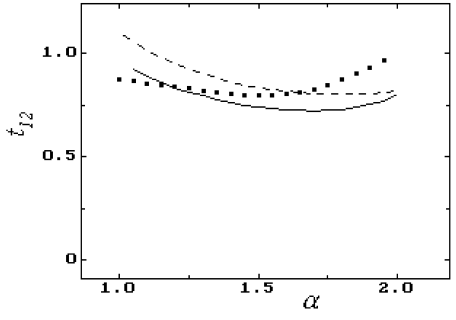

Fig. 5. Bifurcation time t_{12} versus Lévy exponent α at external potential exponent $c = 4.0$. Black dots: bifurcation time deduced from the numerical solution of the fractional Fokker–Planck equation (18) using the Grünwald–Letnikov representation of the fractional Riesz derivative (see appendix). Dashed line: first approximation $t_{12}^{(1)}$; solid line: second approximation $t_{12}^{(2)}$.

equation (18) shown as the dotted line. The second order iteration for the PDF, $\hat{f}_2(k, t)$, can be obtained with `maple6`, from which, in turn, the second approximation for the bifurcation time is found in analogy to above procedure. The result is displayed as the full line in Fig. 5. The two approximate results show in fact surprisingly good agreement with the numerical result of the full PDF. Note that the second approximation appears somewhat worse than the first, however, it captures the minimum of the t_{12} behaviour over α.

3.4. Proof of Non-Unimodality of Stationary Solution for $c > 2$

In this subsection we demonstrate that the stationary solution of the kinetic Eq. (18) has a non-unimodal shape. For this purpose, we use an alternative expression for the fractional Riesz derivative (compare, e.g., ref. 27),

$$\frac{d^\alpha f(x)}{d\,|x|^\alpha} \equiv \Gamma(1+\alpha)\,\frac{\sin(\alpha\pi/2)}{\pi}\int_0^\infty d\xi\,\frac{f(x+\xi)-2f(x)+f(x-\xi)}{\xi^{1+\alpha}} \tag{58}$$

valid for $0 < \alpha < 2$. In the stationary state ($\partial f/\partial t = 0$), we get from Eq. (18):

$$\frac{d}{dx}\,(\mathrm{sgn}(x)\,|x|^{c-1}\,f_{\mathrm{st}}) + \frac{d^\alpha f_{\mathrm{st}}}{d\,|x|^\alpha} = 0. \tag{59}$$

Thus, it follows that at $c > 2$ (strict inequality)

$$\left.\frac{d^\alpha f_{\mathrm{st}}}{d\,|x|^\alpha}\right|_{x=0} = 0, \tag{60}$$

or, from definition (58) and taking into account that $f_{\mathrm{st}}(x)$ is an even function,

$$\int_0^\infty d\xi\,\frac{f_{\mathrm{st}}(\xi)-f_{\mathrm{st}}(0)}{\xi^{1+\alpha}} = 0. \tag{61}$$

From this latter relation, we can immediately obtain proof of the non-unimodality of f_{st}, which we produce in two steps:

(1) If we assume that the stationary PDF $f_{\mathrm{st}}(x)$ is unimodal, then due to the symmetry $x \to -x$, it necessarily has one global maximum at $x = 0$. In this case the integrand in Eq. (61) must be negative, and therefore contradicts Eq. (61). Therefore, $f_{\mathrm{st}}(x)$ is non-unimodal.

(2) We can in addition exclude $f(0) = 0$, as in this case the integrand will be positive, which is again in contradiction with Eq. (61).

Since $f(x) \to 0$ at $x \to \infty$, basing on statements (1) and (2), one may conclude that the simplest situation is such that $\xi_0 > 0$ exists with the property

$$\int_{\xi_0}^{\infty} d\xi \, \frac{f(\xi) - f(0)}{\xi^{1+\alpha}} < 0, \tag{62}$$

and,

$$\int_{0}^{\xi_0} d\xi \, \frac{f(\xi) - f(0)}{\xi^{1+\alpha}} > 0, \tag{63}$$

i.e., the condition for two-hump stationary PDF for all $c > 2$. At intermittent times, however, we will show that also a trimodal state may exist.

3.5. Power-Law Asymptotics of Stationary Solutions for $c \geqslant 2$, and Finite Variance for $c > 2$

We now derive the power-law asymptotics of the stationary PDF $f_{st}(x)$ for external potentials of the form (5) with general $c \geqslant 2$. To this end, we note that at $x \to +\infty$, it is reasonable to assume

$$\mathbf{D}_{-}^{\alpha} f_{st} \ll \mathbf{D}_{+}^{\alpha} f_{st}, \tag{64}$$

since the region of integration for the right-side Riemann–Liouville derivative $(\mathbf{D}_{-}^{\alpha} f_{st})(x)$, (x, ∞), is much smaller than the region of integration for the left-side derivative $(\mathbf{D}_{+}^{\alpha} f_{st})(x)$, $(-\infty, x)$, in which also the major portion of $f_{st}(x)$ is located. Thus, at large x we get for the stationary state,

$$\frac{d}{dx}\left(\frac{dU}{dx} f_{st}\right) - \frac{1}{2\cos(\pi\alpha/2)} \frac{d^2}{dx^2} \int_{-\infty}^{x} \frac{f_{st}(\xi)\, d\xi}{(x-\xi)^{a-1}} \cong 0. \tag{65}$$

Equivalently, this corresponds to the approximative equality

$$x^{c-1} f_{st}(x) \cong \frac{1}{2\cos(\pi\alpha/2)} \frac{d}{dx} \int_{-\infty}^{x} \frac{f_{st}(\xi)\, d\xi}{(x-\xi)^{a-1}}. \tag{66}$$

We are seeking asymptotic behaviours of $f_{st}(x)$ in the form $f(x) \approx C_1 / x^{\mu}$ $(x \to +\infty, \mu > 0)$. After integration of relation (66), we find

$$\frac{2C_1 \cos(\pi\alpha/2)\, \Gamma(2-\alpha)}{-\mu + c} x^{-\mu+c} \cong \int_{-\infty}^{x} \frac{f_{st}(\xi)\, d\xi}{(x-\xi)^{a-1}}. \tag{67}$$

The integral on the right hand side can be approximated through

$$\frac{1}{x^{\alpha-1}}\int_{-\infty}^{x} f_{\mathrm{st}}(\xi)\,d\xi \cong \frac{1}{x^{\alpha-1}}\int_{-\infty}^{\infty} f_{\mathrm{st}}(\xi)\,d\xi = \frac{1}{x^{\alpha-1}}. \tag{68}$$

Thus, we identify the powers of x and the prefactor, with the results

$$\mu = \alpha + c - 1 \tag{69}$$

and

$$C_1 = \frac{\sin(\pi\alpha/2)\,\Gamma(\alpha)}{\pi}. \tag{70}$$

By symmetry of the PDF we therefore recover the general asymptotic form

$$f(x) \approx \frac{\sin(\pi\alpha/2)\,\Gamma(\alpha)}{\pi\,|x|^{\mu}}, \qquad x \to +\infty \tag{71}$$

for all $c \geqslant 2$. This result is remarkable, for various reasons:

(i) despite the approximations involved, the asymptotic form (71) for arbitrary $c \geqslant 2$ matches exactly previously obtained forms, such as the exact analytical result for the harmonic LF (linear Lévy oscillator), $c = 2$ reported in ref. 32; the result for the quartic Lévy oscillator with $c = 4$ discussed in refs. 34 and 35; and the case of even power-law exponents $c = 2m+2$ ($m \in \mathbb{N}_0$) given in ref. 34.

(ii) The prefactor C_1 is independent of the potential exponent c; in this sense, C_1 is universal.

(iii) For each value α of the Lévy index the "critical" value

$$c_{\mathrm{cr}} = 4 - \alpha \tag{72}$$

exists such that at $c < c_{\mathrm{cr}}$ the variance $\langle x^2 \rangle$ is infinite, whereas at $c > c_{\mathrm{cr}}$ the variance is *finite*.

(iv) We have found a fairly simple trick to construct stationary solutions at large x in the form of inverse power series.

4. NUMERICAL RESULTS

In this section, we show results for the PDF of the fractional Fokker–Planck equation (18) obtained via two different numerical techniques, one

being the Grünwald–Letnikov method, which is based on an iterative solution of the deterministic dynamical equation (18) by replacing the Riesz fractional derivative with Grünwald–Letnikov operators; the other being the Langevin method, in which the Langevin equation with Lévy noise, Eq. (6) is integrated numerically. Both methods lead to analogous results, and they also produce results for the PDF which are in perfect agreement with above analytical results. We present the numerical results in two subsections, devoted to the two numerical methods. These methods themselves are discussed in the appendix.

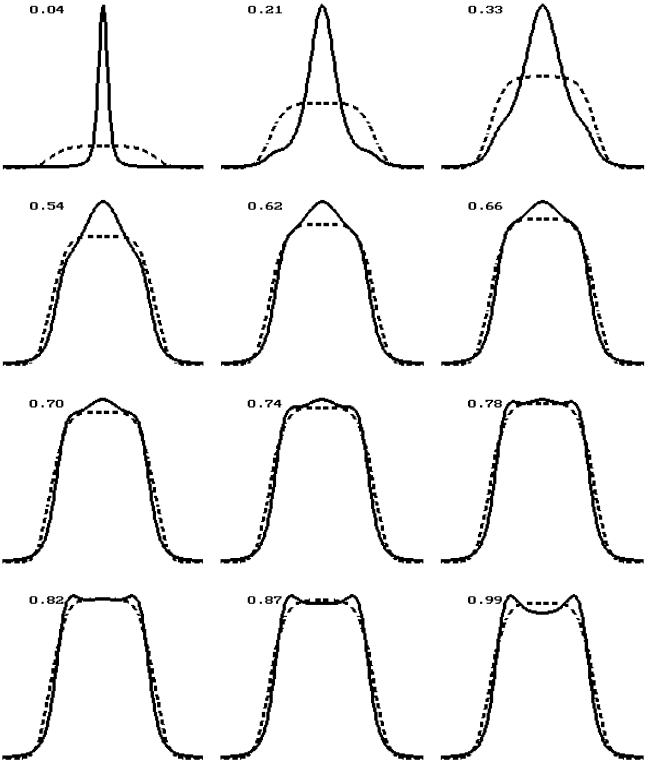

Fig. 6. Time evolution of the PDF governed by the fractional Fokker–Planck equation (18) in a superharmonic potential (5) with exponent $c = 5.5$, and for Lévy index $\alpha = 1.2$; obtained from numerical solution using the Grünwald–Letnikov method explained in the appendix. Initial condition is $f(x, 0) = \delta(x)$. The thin lines indicate the corresponding Boltzmann distribution. The transitions between $1 \to 3 \to 2$ humps are clearly seen. This picture of time evolution is typical for $c > 4$. On a finer scale, we depict the transient trimodal state in Fig. 7.

4.1. Results from the Grünwald–Letnikov Method

4.1.1. Trimodal Transient State at $c > 4$

Before, we have proved the existence of a bimodal stationary state for the quartic ($c = 4$) Lévy oscillator. This bimodality emerges as a bifurcation at a critical time t_{cr}, at which the curvature at the origin vanishes. This scenario is replaced for $c > 4$, as displayed in Fig. 6. Thus, there obviously exist two timescales, the critical time for the emergence of the two off-centre maxima, which are characteristic of the stationary state; and a second one, which corresponds to the relaxing initial central hump, i.e., the decaying initial distribution $f(x, 0) = \delta(x)$. The formation of the two off-centre humps while the central one is still present, is detailed in Fig. 7. This existence of a transient trimodal state was found to be typical for all $c > 4$.

In Figs. 8 and 9, we show additional details of the trimodal state. Thus, Fig. 8 depicts a bifurcation diagram for the process described earlier; the initial monomodal PDF bifurcates to a trimodal one, before it finally becomes bimodal. In Fig. 9, these two turnover times are displayed as

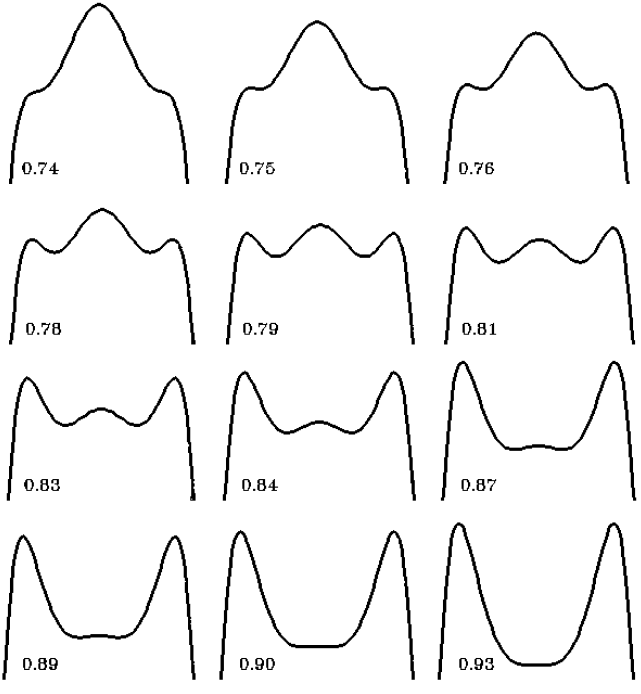

Fig. 7. The transition $1 \to 3 \to 2$ from Fig. 6 on a finer scale ($c = 5.5$, $\alpha = 1.2$).

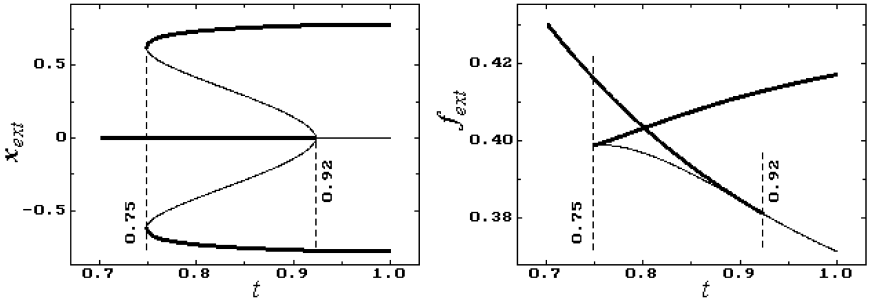

Fig. 8. Bifurcation diagrams for the case $c = 5.5$ and $\alpha = 1.2$ corresponding to Figs. 6 and 7. Left: positions $x_{\max}$ of the maxima (global and local, thick lines); the thin lines indicate the positions of the minima (at the first bifurcation time, there is a horizontal tangent at the site of the two emerging off-centre maxima. The bifurcation times are $t_{13} = 0.75 \pm 0.01$ and $t_{32} = 0.92 \pm 0.01$. Right: values of the PDF at the maxima (thick lines); the thin line indicates the value of the PDF in the minima.

function of the Lévy index α. Clearly, there is always a gap between these two time scales, leaving the intermittent time for the trimodal state, and for $\alpha \to 2$, this region shrinks, both curves converge to infinity, as in the regular Gaussian case no such bifurcation exists.

4.1.2. Phase Diagrams for n-Modal States

The above findings can be put in context with the purely bimodal case discussed earlier. A convenient way of displaying the *n*-modal character of the PDF in the presence of a superharmonic external potential of the type (19) is the phase diagram shown in Fig. 10. There, we summarise

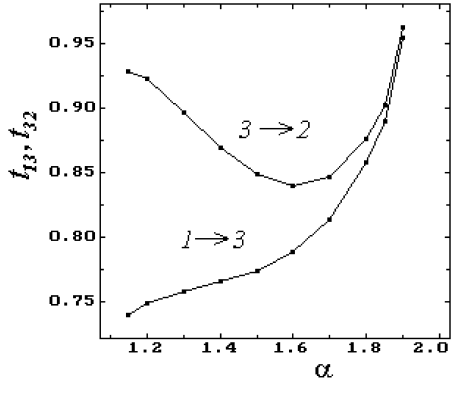

Fig. 9. Bifurcation times t_{13} versus α (lower curve) and t_{32} (upper curve) for the external potential exponent $c = 5.5$.

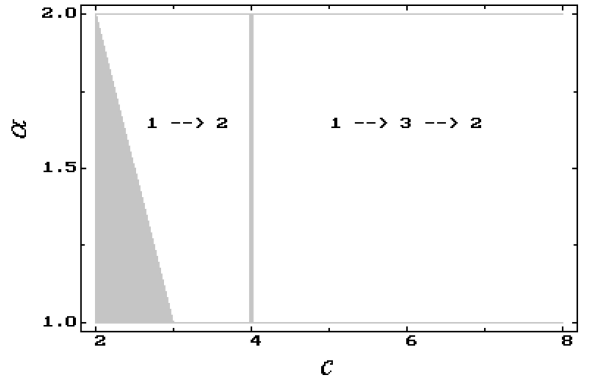

Fig. 10. (c, α)-map showing different regimes of evolution of the PDF, and the stationary states. The region with infinite variance is shaded. The region $c < 4$ covers the transition from 1 to 2 humps during time evolution. For $c > 4$, a transition from 1 to 3, and then from 3 to 2 humps occur. For all c's there are two maxima in the stationary state. Compare Fig. 11.

the findings that for $2 < c \leqslant 4$ the bifurcation occurs between the initial monomodal and the stationary bimodal PDF at a finite critical time, whereas for $c > 4$, a transient trimodal state exists. Moreover, we also include the shaded region, in which c is too small to ensure a finite variance. Complementarily, in Fig. 11, the temporal domains of the n-modal states are graphed, and the solid lines separating these domains correspond to the critical timescales. Again, the transient nature of the trimodal state is distinct.

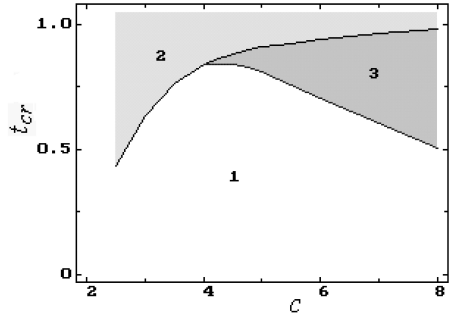

Fig. 11. (c, t)-map showing states with different number of maxima, and the transitions between them during time evolution. Region 1: PDF has 1 hump; region 2: PDF has 2 humps; region 3: PDF has 3 humps. At $c < 4$ there is only a transition $1 \to 2$, whereas at $c > 4$ there are two transitions: $1 \to 3$ and after the transient trimodal regime, $3 \to 2$.

4.2. Langevin Method

As explained in the appendix, this method directly integrates the Langevin equation for white Lévy noise, the latter being portrayed in Fig. 3. Typical results for the sample paths under the influence of an external potential (19) with increasing superharmonicity are shown in Fig. 12 in comparison to the Brownian case (i.e., white Gaussian noise). For increasing external exponent c, the long excursions, which are typical for homogeneous LFs are increasingly suppressed. In the harmonic case

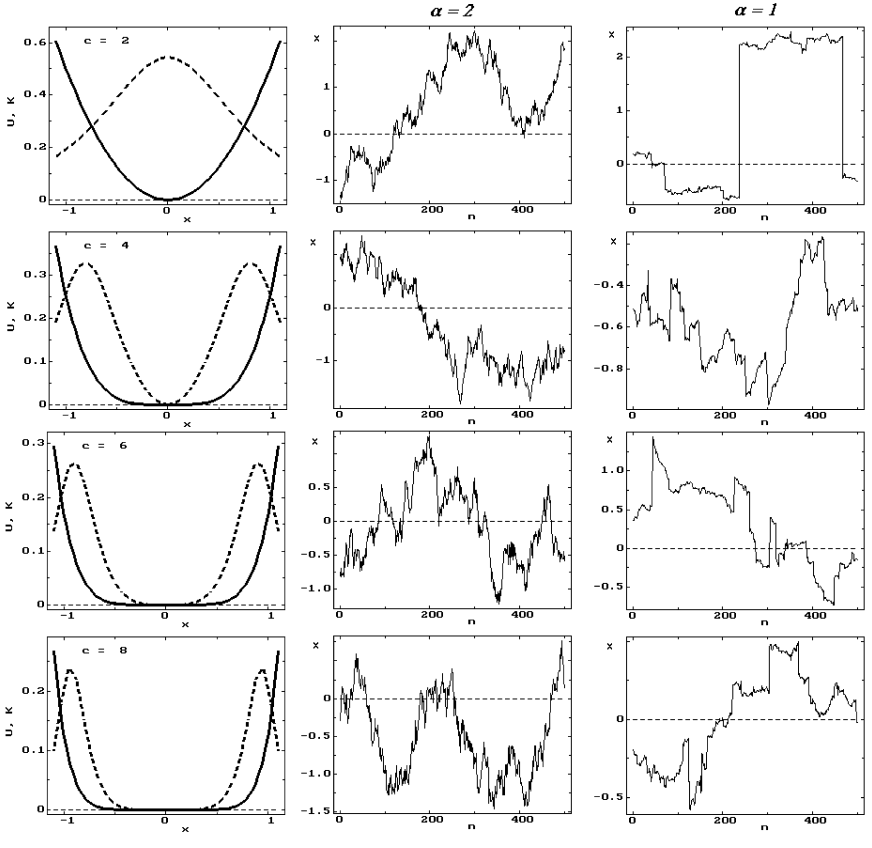

Fig. 12. Left column: the potential energy functions $U = x^c/c$, (solid lines) and their curvatures (dotted lines) for different values of c: $c = 2$ (linear oscillator), and $c = 4, 6, 8$ (strongly nonlinear oscillators). Middle column: typical sample paths of the Brownian oscillators, $\alpha = 2$, with the potential energy functions shown on the left. Right column: typical sample paths of the Levy oscillators, $\alpha = 1$. It is seen that with m increasing the potential walls become steeper, and the Lévy flights become shorter; in this sense, they are "confined."

$c = 2$ still present (in this case, the variance is diverging), they are clearly confined for $c > 2$. Note the comparable ordinate windows in comparison to the significantly different scale in the homogeneous case of Fig. 3. For all displayed cases, however, the qualitative behaviour of the noise under the external potential is different from the Brownian noise even in this case of strong confinement. In the same figure, we also show the curvature of the external potential. Additional investigations have shown that the maximum curvature is always very close to the positions of the two maxima, leading us to conjecture that they are in fact identical.

The latter observation is further investigated in Fig. 13. On a linear scale, the potential well and its curvature are compared to the stationary PDF, clearly demonstrating the proximity of maximum curvature and the two maxima. Figure 13 also corroborates on the basis of the Langevin method the asymptotic inverse power-law behaviour derived in Eq. (71).

Finally, in Fig. 14, we display the time evolution of the PDF in the three different modality-regimes according to Fig. 11. The comparatively noisy result is due to a small number of trajectories used for the statistical average, due to the rather computation intensive program.

5. CONCLUSIONS

By combining analytical and numerical results, we discussed LFs in a superharmonic external potential of power c. Depending on the magnitude of this exponent c, different regimes could be demonstrated. Thus, for $c = 2$, the character of the Lévy noise imprinted on the process, is not changed by the external potential: the resulting PDF has Lévy index α, the same as the noise itself, and will thus give rise to a diverging variance at all times. Conversely, for $c > 2$, the variance becomes finite if only $c > c_{cr} = 4 - \alpha$. This is due to the fact that the PDF leaves the class of Lévy stable PDFs and acquires an inverse power-law asymptotic behaviour with power $\mu = \alpha + c - 1$. Obviously, moments of higher order still diverge. Apart from the finite variance, the PDF is distinguished by the observation that it bifurcates from the initial monomodal to a stationary bimodal state. If $c > 4$, there exists a transient trimodal state. This richness of the PDF both during relaxation and at stationarity, depending on a competition between Lévy noise and steepness of the potential is in contrast to the universal approach to the Boltzmann equilibrium, solely defined by the external potential, in classical diffusion.

One may ask for the exact kinetic reason for the occurrence of the multiple humps. Due to the observation that the non-transient humps seem to coincide with the positions of maximum curvature of the external potential, which at these points changes almost abruptly for larger c from a

rather flat to a very steep slope, one may conclude that the random walker, which is driven towards these flanks by the anomalously strong Lévy diffusivity, is thwarted, thus accumulating close to these points. Apart from this observation, we do not have a more intuitive argument for the existence of the humps and their bifurcations.

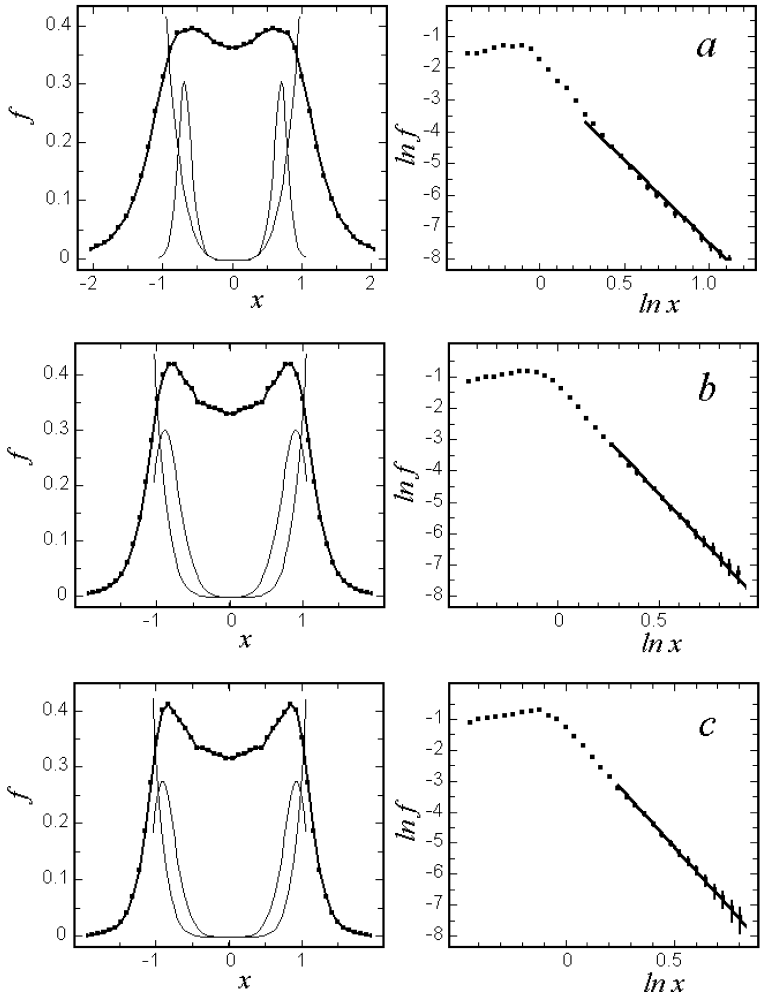

Fig. 13. Stationary PDF $f_{st}(x)$ on linear (left) and double-logarithmic (right) scale, obtained from the Langevin equation for (a) $c = 4.0$, (b) $c = 5.7$, and (c) $c = 6.5$. The thin lines on the left show the potential wells and their curvatures. The solid lines on the right show the asymptotics as given by Eq. (71).

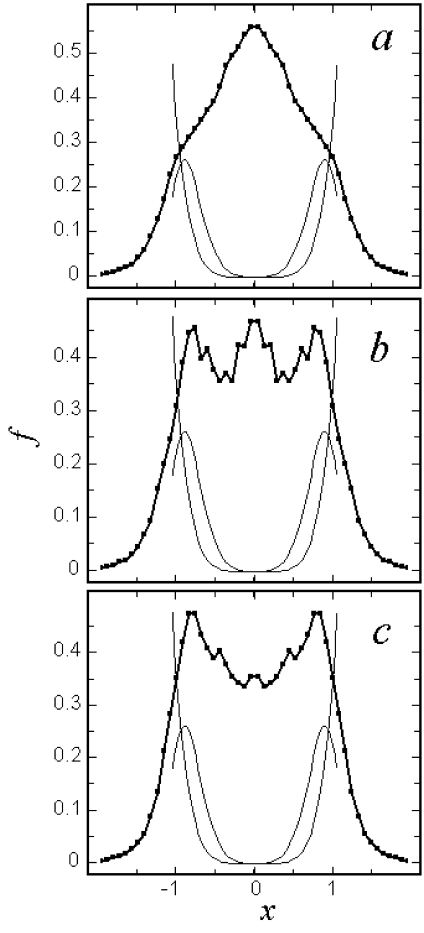

Fig. 14. Time evolution of the PDF $f(x)$ obtained from the Langevin equation for $c = 5.5$, $\alpha = 1.2$; an additional time averaging, together with statistical averaging has been used to present this figures: (a) inside the region of a single peak, $t < t_{13}$ ($t = 0.40 - 0.60$); (b) inside the region of three peaks, $t_{13} < t < t_{32}$ ($t = 0.75 - 0.90$), (c) inside the region of two peaks, $t > t_{32}$ ($t = 1.10 - 1.50$). The regions of time averaging are chosen on the basis of Fig. 11.

The different regimes for $c > 2$ can be classified in terms of critical quantities, in particular, the bifurcation time(s) t_{cr} and the critical external potential exponent c_{cr}. LFs in superharmonic potentials can then be conveniently represented by phase diagrams on the (c, α) and (c, t_{cr}) plains.

The numerical solution of both the fractional Fokker–Planck equation in terms of the Grünwald–Letnikov scheme used to find a discretized approximation of the fractional Riesz operator shows reliable convergence, as corroborated by direct solution of the corresponding Langevin equation.

Our findings have underlined the statement that the properties of LFs, in particular under nontrivial boundary conditions or in an external potential are not fully understood. The general difficulty, which hampers a similarly straightforward investigation as in the regular Gaussian or the subdiffusive cases, is connected with the strong spatial correlations of the problems, manifested in the integrodifferential nature of the Riesz fractional operator. For this reason it is already nontrivial to determine the stationary solution of the process, or its first passage time density.[43] We expect, by the fact that diverging fluctuations appear to be relevant in physical systems, a range of yet unknown properties of LFs remain to be discovered.

APPENDIX A. NUMERICAL SOLUTION METHODS

In this appendix, we briefly review the numerical techniques, which were used in this work to determine the PDF from the fractional Fokker–Planck equation (18) and the Langevin equation (17).

A.1. Numerical Solution of the Fractional Fokker–Planck Equation (18) via the Grünwald–Letnikov Method

From a mathematical point of view, the fractional Fokker–Planck equation (18) is a first-order partial differential equation in time, and of nonlocal, integro-differential kind in the position co-ordinate x. It can be solved numerically via an efficient discretisation scheme following Grünwald and Letnikov.[39–41]

Let us designate the force component on the right hand side of Eq. (18) as

$$\bar{F}(x, t) \equiv \frac{\partial}{\partial x}\left(\frac{dU}{dx} f\right); \tag{A.1}$$

and the diffusion part as

$$\bar{D}(x, t) \equiv \frac{\partial^{\alpha} f}{\partial |x|^{\alpha}}. \tag{A.2}$$

With these definitions, we can rewrite Eq. (18) in terms of a discretisation scheme as

$$\frac{f_{j,n+1} - f_{j,n}}{\Delta t} = \bar{F}_{j,n} + \bar{D}_{j,n}, \tag{A.3}$$

where we encounter the term

$$\bar{F}_{j,n} = x_j^{c-2}\left[(c-1)\, f_{j,n} + x_j \frac{f_{j+1,n} - f_{j-1,n}}{2\,\Delta x}\right], \tag{A.4}$$

which is the force component of the potential $U(x) = |x|^c/c$. Here, Δt and Δx are the finite increments in time and position, such that $t_n = n\,\delta t$ and $x_j = j\,\Delta x$, for $n = 0, 1, \ldots, N$ and $j = 0, 1, \ldots, J$, and $f_{j,n} \equiv f(x_j, t_n)$. Due to the inversion symmetry of the kinetic equation (18), it is sufficient to solve it on the right semi-axis. In the evaluation of the numerical scheme, we define x_J such that the PDF in the stationary state is sufficiently small, say, 10^{-3}, as determined from the asymptotic form (71).

In order to find a discrete time and position expression for the fractional Riesz derivative in Eq. (A.2), we employ the Grünwald–Letnikov scheme,[39–41] according to which we obtain

$$\bar{D}_{j,n} = -\frac{1}{2(\Delta x)^\alpha \cos(\pi\alpha/2)} \sum_{q=0}^{J} \xi_q [f_{j+1-q,n} + f_{j-1+q,n}] \tag{A.5}$$

where

$$\xi_q = (-1)^q \binom{\alpha}{q}, \tag{A.6}$$

with

$$\binom{\alpha}{q} = \begin{cases} \alpha(\alpha-1)\cdots(\alpha-q+1)/q!, & q > 0 \\ 1, & q < 0, \end{cases} \tag{A.7}$$

and $1 < \alpha \leqslant 2$. Note that in the limiting case $\alpha = 2$ only three coefficients differ from zero, namely, $\xi_0 = 1$, $\xi_1 = -2$, and $\xi_2 = 1$, corresponding to the standard three-point difference-scheme for the second order derivative, $d^2g(x_j)/dx^2 \approx (g_{j+1} - 2g_j + g_{j-1})/(\Delta x)^2$. In Fig. 15, we demonstrate that with decreasing α, an increasing number of coefficients contribute significantly to the sum in Eq. (A.5). This becomes particularly clear in the logarithmic representation in the bottom plot of Fig. 15. We note that the condition

$$\mu \equiv \Delta t/(\Delta x)^\alpha < 0.5 \tag{A.8}$$

is needed to ensure the numerical stability of the discretisation scheme. In our numerical evaluation, we use $\Delta x = 10^{-3}$, and therefore the associated

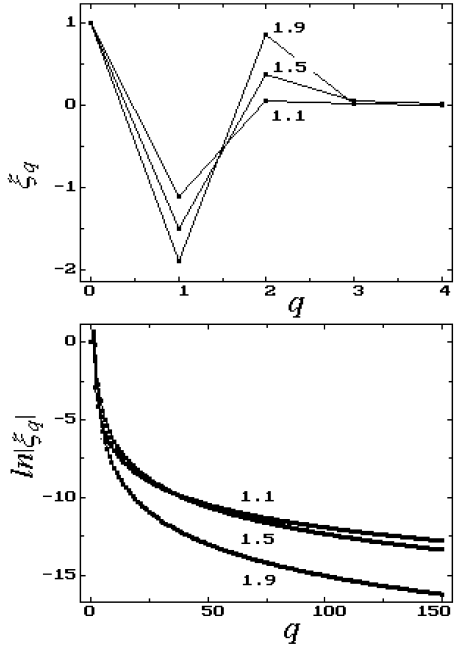

Fig. 15. Coefficients ξ_q in Grünwald–Letnikov approximation for different values of the Lévy index $\alpha = 1.9$, 1.5, and 1.1.

time increment $\Delta t \sim 10^{-5} \cdots 10^{-6}$, depending on the actual value of α. The initial condition for Eq. (A.3) is $f_{0,0} = 1/\Delta x$.

In Fig. 16, the time evolution of the PDF is shown together with the evolution of the force and diffusion components defined by Eqs. (A.1) and (A.2), respectively. Accordingly, at the initial stage of the relaxation process, the diffusion component prevails. The force term grows in the course of time, until at the stationary state $\bar{F} \to -\bar{D}$. This is particularly visible at the bottom right part of Fig. 16, which corresponds to the stationary bimodal state shown to the left.

A.2. Numerical Solution of the Langevin Equation (6)

An alternative way to obtain the PDF is to sample the trajectories determined by the Langevin equation (6). To this end, Eq. (17) is discretized in time according to

$$x_{n+1} = x_n + F(x_n)\,\Delta t + (\Delta t)^{1/\alpha}\, Y_\alpha(n\,\Delta t), \tag{A.9}$$

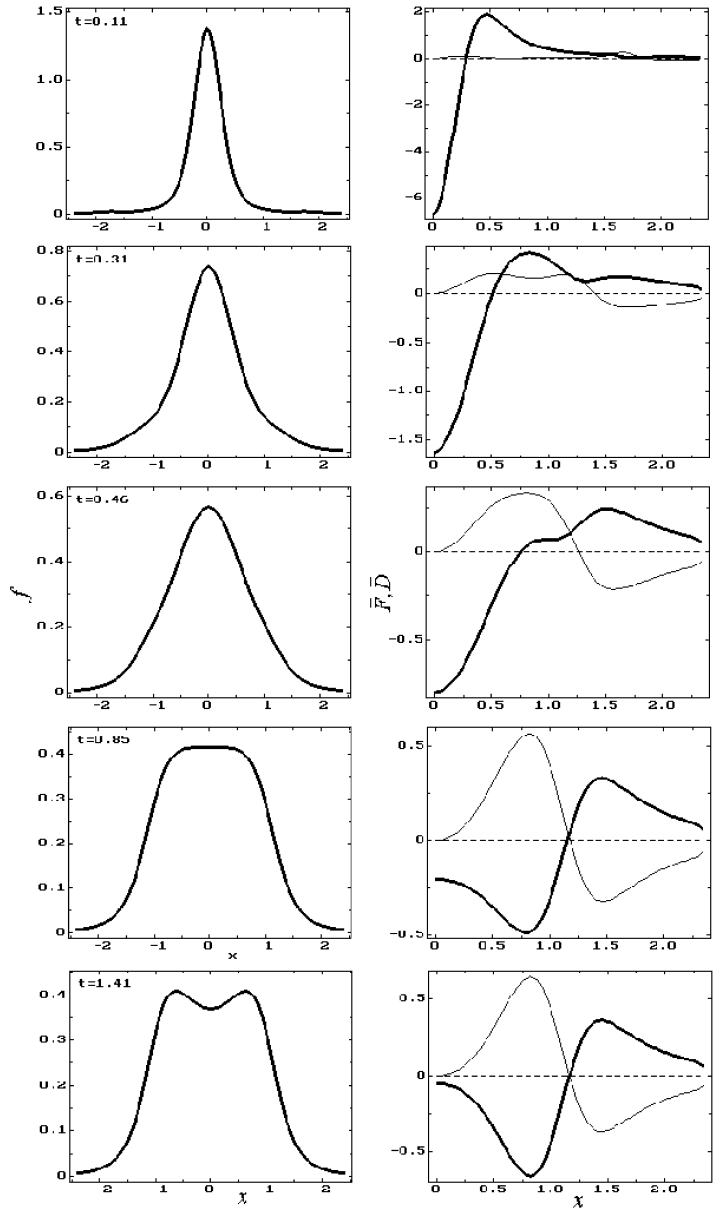

Fig. 16. Further details of the Grünwald–Letnikov scheme. Left: Time evolution of the PDF as obtained by numerical solution of Eq. (A.3) at $c = 4$ and $\alpha = 1.2$. Right: Time evolution of the diffusion component (A.2) (thick lines), and the force term (A.1) (thin lines).

with $t_n = n\,\Delta t$ for $n = 0, 1, 2, \ldots$, and where the force $F(x_n)$ is the dimensionless force field at position x_n. The sequence $\{Y_\alpha(n\,\Delta t)\}$ is a discrete-time approximation of a white Lévy noise of index α with a unit scale parameter. That is, the sequence of independent random variables possessing the characteristic function $\hat{p} = \exp(-|k|^\alpha)$. To generate this sequence $\{Y_\alpha(n\,\Delta t)\}$, we used the method outlined in ref. 42.

ACKNOWLEDGMENTS

The authors thank F. Mainardi and R. Gorenflo for stimulating discussions and G. Voitsenya for help in numerical simulation. A.C. acknowledges NORDITA for hospitality. This work is supported by the INTAS Project 00-0847.

REFERENCES

1. B. D. Hughes, *Random Walks and Random Environments, Vol. 1: Random Walks* (Oxford University Press, Oxford, 1995). Note that Hughes coins the term "leapers" for LFs.
2. J.-P. Bouchaud and A. Georges, *Phys. Rep.* **88**:127 (1990).
3. P. Lévy, *Théorie de l'addition des variables aléatoires* (Gauthier-Villars, Paris, 1954).
4. B. V. Gnedenko and A. N. Kolmogorov, *Limit Distributions for Sums of Random Variables* (Addison–Wesley, Reading, 1954)
5. J. Klafter, M. F. Shlesinger, and G. Zumofen, *Phys. Today* **49**:33 (1996).
6. S. Chandrasekhar, *Rev. Mod. Phys.* **15**:1 (1943).
7. N. G. van Kampen, *Stochastic Processes in Physics and Chemistry* (North-Holland, Amsterdam, 1981).
8. G. Zumofen and J. Klafter, *Chem. Phys. Lett.* **219**:303 (1994).
9. H. Katori, S. Schlipf, and H. Walther, *Phys. Rev. Lett.* **79**:2221 (1997).
10. A. V. Chechkin, V. Y. Gonchar, and M. Szydlowsky, *Phys. Plasma* **9**:78 (2002).
11. A. Carati, L. Galgani, and B. Pozzi, *Phys. Rev. Lett.* **90**:010601 (2003).
12. M. Levandowsky, B. S. White, and F. L. Schuster, *Acta Protozool.* **36**:237 (1997).
13. G. M. Viswanathan, V. Afanasyev, S. V. Buldyrev, E. J. Murphey, P. A. Prince, and H. E. Stanley, *Nature* **381**:413 (1996).
14. G. Ramos-Fernandez, J. L. Mateos, O. Miramontes, G. Cocho, H. Larralde, and B. Ayala-Orozco, preprint cond-mat/0301019.
15. B. B. Mandelbrot, *J. Bus.* **36**:394 (1963); *ibid.* **39**:242 (1966); *ibid.* **40**:393 (1967); compare R. N. Mantegna and H. E. Stanley, *J. Stat. Phys.* **89**:469 (1997); J.-P. Bouchaud and D. Sornette, *J. Phys. (Paris) I* **4**:863 (1994).
16. D. Brockmann and T. Geisel, *Phys. Rev. Lett.* **90**:170601 (2003).
17. I. Eliazar and J. Klafter, *J. Stat. Phys.* **111**:739 (2003).
18. J. Klafter, A. Blumen, and M. F. Shlesinger, *Phys. Rev. A* **35**:3081 (1987).
19. I. M. Sokolov and R. Metzler, *Phys. Rev. E* **67**:010101(R) (2003).
20. V. Seshadri and B. J. West, *Proc. Natl. Acad. Sci. USA* **79**:4501 (1982); B. J. West and V. Seshadri, *Physica A* **113**:203 (1982).
21. H. C. Fogedby, *Phys. Rev. Lett.* **73**:2517 (1994); *Phys. Rev. E* **58**:1690 (1998).
22. J. Honkonen, *Phys. Rev. E* **53**:327 (1996).

23. A. V. Chechkin and V. Yu. Gonchar, *J. Eksper. Theor. Phys.* **91**:635 (2000); V. V. Yanovsky, A. V. Chechkin, D. Schertzer, and A. V. Tur, *Physica A* **282**:13 (2000).
24. F. Peseckis, *Phys. Rev. A* **36**:892 (1987).
25. R. Metzler and J. Klafter, *Phys. Rep.* **339**:1 (2000).
26. I. M. Sokolov, J. Klafter, and A. Blumen, *Phys. Today* **55**:48 (2002).
27. S. G. Samko, A. A. Kilbas, and O. I. Marichev, *Fractional Integrals and Derivatives, Theory, and Applications* (Gordon & Breach, New York, 1993).
28. W. R. Schneider, in *Stochastic Processes in Classical and Quantum Systems*, Lecture Notes in Physics, Vol. 262, S. Albeverio, G. Casati, and D. Merlini, eds. (Springer-Verlag, Berlin, 1986).
29. D. Kusnezov, A. Bulgac, and G. D. Dang, *Phys. Rev. Lett.* **82**:1136 (1999).
30. R. Metzler, *Phys. Rev. E* **62**:6233 (2000).
31. E. Lutz, *Phys. Rev. Lett.* **86**:2208 (2001).
32. S. Jespersen, R. Metzler, and H. C. Fogedby, *Phys. Rev. E* **59**:2736 (1999).
33. I. Sokolov, J. Klafter, and A. Blumen, *Phys. Rev. E* **64**:021107 (2001).
34. A. Chechkin, V. Gonchar, J. Klafter, R. Metzler, and L. Tanatarov, *Chem. Phys.* **284**:233 (2002).
35. A. V. Chechkin, J. Klafter, V. Yu. Gonchar, R. Metzler, and L. V. Tanatarov, *Phys. Rev. E* **67**:010102(R) (2003).
36. F. Mainardi, Yu. Luchko, and G. Pagnini, *Fract. Calc. Appl. Anal.* **4**:153 (2001).
37. R. Balescu, *Equilibrium and Nonequilibrium Statistical Mechanics*, Vol. II (Wiley, New York, 1975).
38. A more formal way of writing this Langevin equation is
$$x(t+dt)-x(t)=-\frac{1}{m\gamma}\frac{dU(x)}{dx}\,dt+D^{1/\alpha}Y_\alpha(dt).$$
39. I. Podlubny, *Fractional Differential Equations* (Academic Press, San Diego, CA, 1998).
40. R. Gorenflo, in *Fractals and Fractional Calculus in Continuum Mechanics*, A. Carpinteri and F. Mainardi, eds. (Springer, Wien, 1997).
41. R. Gorenflo, F. Mainardi, D. Moretti, G. Pagnini, and P. Paradisi, *Chem. Phys.* **284**:521 (2002).
42. A. V. Chechkin and V. Yu. Gonchar, *Physica A* **27**:312 (2000).
43. J Klafter and L. V. Tanatarov, *J. Phys. A* **36**:L537 (2003).